RSC Mechanochemistry

ROYAL SOCIETY OF CHEMISTRY

PAPER

View Article Online
View Journal | View Issue



Cite this: *RSC Mechanochem.*, 2025, **2**, 127

# Mechanochemical coupling of two coupled kinesin monomers: comparison with that of the single dimer†

Ping Xie *

The dynamics of cargo transport by two coupled kinesin monomers, such as kinesin-1, kinesin-2 and kinesin-3, is studied theoretically and is compared with that by the corresponding single dimer on the basis of our proposed model for the mechanochemical coupling of the two coupled monomers and that of the single dimer. It is shown that if the stalk, which connects the monomer and cargo, has a short length $L_S$ (*e.g.*, $L_S$ < 5 nm) the cargo transport by the two monomers can be efficient with an unloaded velocity that can be similar to that by the corresponding single dimer, whereas the cargo transport by the two monomers with a long $L_S$ can only be inefficient with an unloaded velocity and a stall force much smaller than those with the short $L_S$. Although the unloaded velocity for the two coupled kinesin-1 monomers with a short $L_S$ can be similar to that for the single kinesin-1 dimer, the stall force for the former is reduced by about 2 times relative to that for the latter. The dynamics of the two coupled kinesin-3 KIF1A monomers relative to the single kinesin-3 dimer is similar to that of the two coupled kinesin-1 monomers relative to the single kinesin-1 dimer. By contrast, the stall force for the two kinesin-2 KIF3A monomers with a short $L_S$ can be similar to that for the single kinesin-2 KIF3AA, KIF3BB or KIF3AB dimer. The theoretical results agree well with the available experimental evidence. The underlying mechanism of the two coupled kinesin-1 or kinesin-3 monomers with the short $L_S$ having an evidently smaller stall force than the corresponding single dimer and the two coupled kinesin-2 KIF3A monomers with the short $L_S$ having a stall force similar to that of the corresponding single dimer is explained.

Received 28th May 2024
Accepted 13th November 2024

DOI: 10.1039/d4mr00057a

rsc.li/RSCMechanochem



## 1. Introduction

Cytoskeletal molecular motors are important classes of proteins that play critical roles in transport of cargos such as organelles and many other subcellular materials within cells. Kinesin-1, kinesin-2 and kinesin-3 proteins are typical examples of these molecular motors that make use of the chemical energy of ATP hydrolysis to move progressively along microtubule (MT) filaments towards the plus end.[1–7] Using various methods, and in particular using single-molecule optical trapping techniques, the dynamics of the single kinesin motors has been studied extensively.[8–10] For example, a kinesin-1 motor can move with a velocity of about 1 μm $s^{-1}$ under no load and can give a maximum driving force or a stall force of about (6 ∼ 8) pN. It was found that in cells a cargo is often transported by multiple molecular motors.[11,12] Thus, the cargo transport by multiple coupled kinesin motors has also attracted much attention both theoretically and experimentally.[13–23] It was found that the transport by multiple kinesin motors has advantages over that by a single one. For example, while the velocity of the two coupled kinesin motors under no load is similar to that of the single one, the run length of the former under no load is longer than that of the latter and the stall force of the former is larger than that of the latter.[21–28]

Besides the cargo transport by multiple coupled kinesin dimers, several research studies on the cooperative transport by multiple single-headed kinesin motors (or kinesin monomers) have also been presented.[29–33] Recently, using a combination of *in vitro* and cellular assays Schimert *et al.*[34] elaborately studied the cargo transport by multiple coupled kinesin monomers, such as kinesin-1, kinesin-2 and kinesin-3, with different lengths of the stalk connecting the monomers and cargo and compared it with that by the corresponding dimers. Interestingly, they found that the monomers, which are not processive as individuals, can work cooperatively to drive a cargo to move efficiently and continuously towards the MT plus end when the stalk is short. However, the force output by multiple kinesin-1 (or kinesin-3) monomers was evidently smaller than that by multiple corresponding dimers. By contrast, the force output by multiple kinesin-2 KIF3A monomers was similar to that by multiple coupled KIF3AB dimers. More puzzlingly, the

*Laboratory of Soft Matter Physics, Institute of Physics, Chinese Academy of Sciences, Beijing 100190, China. E-mail: pxie@aphy.iphy.ac.cn*

† Electronic supplementary information (ESI) available. See DOI: https://doi.org/10.1039/d4mr00057a

transport velocity and force output by multiple monomers decreased significantly as the stalk length increased, whereas the stalk length had little effect on the transport velocity and force output by the dimers. However, how the multiple coupled monomers with a short stalk can drive the cargo to move efficiently is unclear. The underlying mechanism of the force output by multiple kinesin-1 (or kinesin-3) monomers being evidently smaller than that by multiple corresponding dimers and the force output by multiple kinesin-2 KIF3A monomers being similar to that by multiple kinesin-2 KIF3AB dimers is not known. How does the stalk length affect significantly the cargo transport by multiple coupled monomers?

Theoretically, the studies of cargo transport by multiple coupled kinesin monomers were performed based on a two-state ratchet model for a single monomer, where the interaction potential of the monomer with a tubulin heterodimer was required to have an asymmetric form along the MT filament.[35–39] The effect of the stalk length on the dynamics of the system has not been considered in these theoretical studies. Moreover, these theoretical studies predicted that the cargo transport by

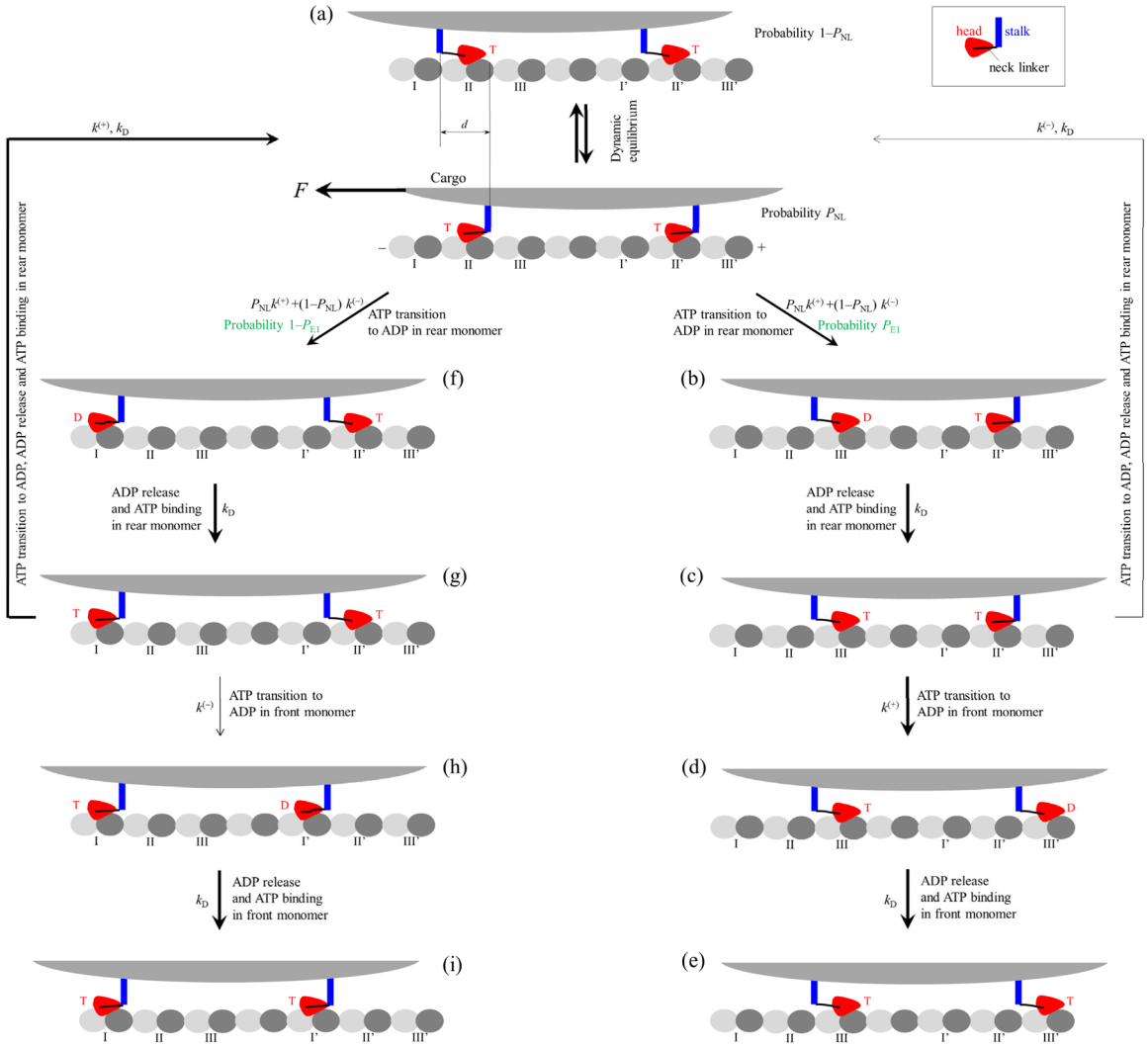


Fig. 1 Schematic illustration of the cargo transport by two coupled kinesin-1 monomers with a short stalk under a backward load $F$ on the cargo. (a)–(i) Mechanochemical pathway at saturating ATP concentrations (see Section 2.1 for detailed descriptions). Here, only the state transitions of the system occurring after the ATP transition of ADP in the rear monomer in (a) are shown. The thickness of the arrow represents the relative magnitude of the probability of the transition between the two states connected by the arrow under a low $F$. At saturating ATP concentrations the rate of ATP binding is considered to be infinitely large. Since ADP release from the MT-bound monomer is a non-rate-limiting step of the ATPase activity, it is considered that ADP release from the ADP-monomer occurs before the ATP transition to ADP in another monomer with the NL in the forward orientation. $P_{NL}$ stands for the probability of the two monomers in the state with docked NLs (the lower panel) in (a), $P_{E1}$ stands for the probability of the transition from (a) to (b) and correspondingly $1 - P_{E1}$ is the probability of the transition from (a) to (f), $k^{(+)}$ and $k^{(-)}$ stand for the rates of the ATP transition to ADP of the monomer with its NL in the forward and backward orientations, respectively, $k_D$ stands for the rate of ADP release from the ADP-head bound to MT (with $k_D \gg k^{(+)}$ and $k^{(-)}$), and $P_{NL}k^{(+)} + (1 - P_{NL})k^{(-)}$ is the overall rate of the ATP transition to ADP in one monomer in (a). Since the diffusion of the monomer from the local tubulin to the adjacent tubulin, which occurs after the ATP transition to ADP in the monomer, is on the timescale <1 μs, which is much shorter than the inverse of the rate constant of the ATPase activity, the rate of the diffusion is not indicated here.

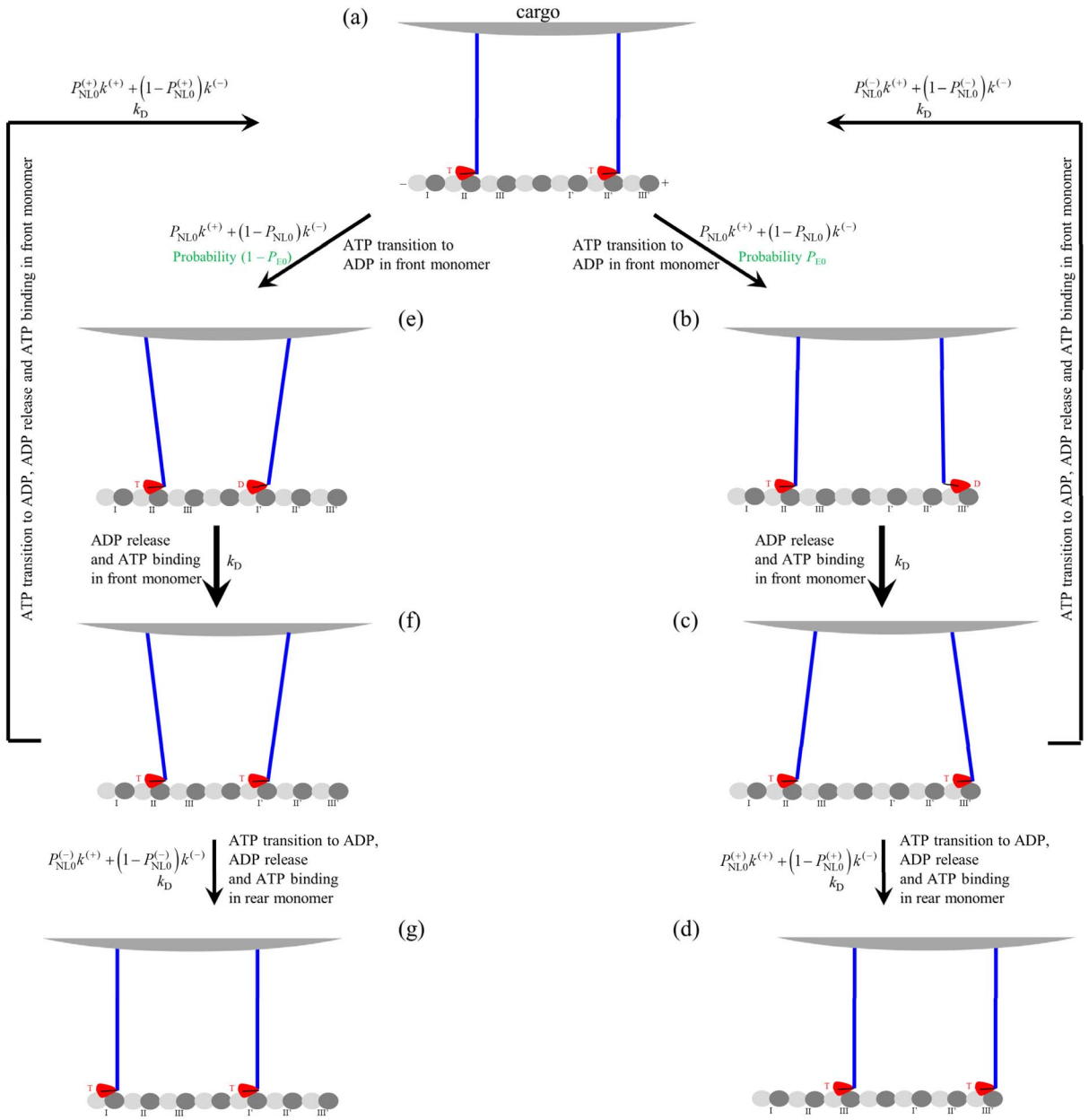


Fig. 2 Schematic illustration of the cargo transport by two coupled kinesin-1 monomers with a long stalk. (a)–(g) Mechanochemical pathway at saturating ATP concentrations (see Section 2.2 for detailed descriptions). Note that the NL of the ATP-monomer can be mainly in the docked form or can be occasionally in the undocked form, and for simplicity, only the docked NL is shown here. Here, only the state transitions of the system occurring after the ATP transition of ADP in the front monomer in (a) are shown. The thickness of the arrow represents the relative magnitude of the probability of the transition between the two states connected by the arrow under no load. At saturating ATP concentrations the rate of ATP binding is considered to be infinitely large. Since ADP release from the MT-bound monomer is a non-rate-limiting step of the ATPase activity, it is considered here that ADP release from the ADP-monomer occurs before the ATP transition to ADP in another monomer. Since the diffusion of the monomer from the local tubulin to the adjacent tubulin, which occurs after the ATP transition to ADP in the monomer, is on the timescale <1 μs, which is much shorter than the inverse of the rate constant of the ATPase activity, the rate of the diffusion is not indicated here.

multiple monomers has a small velocity similar to that by the single monomer, which is inconsistent with the experimental data of Schimert *et al.*[34]

In this work, based on the model for the mechanochemical coupling of the kinesin dimer presented before[40,41] (also see ESI text and Fig. S1†), a model for the mechanochemical coupling of the cargo transport by two coupled monomers is presented (see Model and Fig. 1 and 2), where the interaction potential between a monomer and a tubulin is not required to have an asymmetric form. With the model, we theoretically study the cargo transport by two coupled monomers, addressing the aforementioned unclear issues. Since both the cargo transport

by two coupled monomers and that by a dimer involve two kinesin heads, it is interesting to compare the dynamics of the two coupled monomers with that of the single dimer. Thus, we first study the dynamics of the single dimer theoretically, as done before.[40–42] With the parameter values determined by fitting the theory to the available single-molecule experimental data for the single dimer, we then theoretically study the dynamics of the two coupled monomers. The theoretical results well explain the available experimental data.[34] The underlying mechanism of the distinction in the dynamics between the two coupled kinesin-1 (or kinesin-3) monomers with a short stalk and the corresponding single dimer is due to the difference in the stepping manner of the two heads and the ATPase rate of the head with its neck linker (NL) in the forward (plus-end) orientation being much higher than that with its NL in the backward orientation. For the former, the two heads step in an inchworm manner while for the latter the two heads step in a hand-over-hand manner. The hand-over-hand stepping manner ensures that the NLs of the trailing and leading heads in the ATP state are always in the forward and backward orientations under any backward load, respectively, resulting in a higher stall force. By contrast, the inchworm stepping manner does not ensure that the NLs of the two heads in the ATP state are always in the forward orientation, resulting in a smaller stall force.

## 2. Model

As done for the dimer[40–42] (also see ESI text†), the model for the mechanochemical coupling of the two coupled monomers is developed on the basis of the following three elements. (1) A monomer has a weak interaction with MT in the ADP state and a strong interaction in other nucleotide states.[43–45] The strong and weak interactions induce respectively large and little conformational changes of the local tubulin, as structural studies indicated.[46–49] The ADP-monomer has a much lower affinity ($E_{w1}$) to the tubulin having large conformational changes than the affinity ($E_{w2}$) to the tubulin having little conformational changes, as all-atom molecular dynamics simulations showed.[47,48] Hence, after the monomer transitions from ATP to ADP state, a short time $t_r$ (on the order of 10 μs) is present when the local tubulin retains the large conformational changes, with the affinity ($E_{w1}$) of the ADP-monomer to the local tubulin being much smaller than the affinity ($E_{w2}$) to other tubulins. After time $t_r$, the local tubulin returns elastically to the normal unchanged form, with the affinity of the ADP-monomer to the local tubulin becoming the same as the affinity ($E_{w2}$) to other tubulins. The evidence that kinesin can induce the conformational changes of MT, which in turn can affect the MT-affinity of kinesin, is also supported by recent studies showing that the motility of a kinesin-4 can be affected by other kinesins far away on the MT filament.[49–51] (2) In the ATP or ADP Pi state, the monomer can have a large conformational change with its flexible NL docking in the forward orientation relative to that in the ADP or nucleotide-free ($\phi$) state (see ESI text† for details). (3) The kinesin-1 or kinesin-3 monomer with the NL in the forward orientation has a much higher rate of ATP transition to ADP than that with the NL not in the forward orientation, as explained in the following part. The structural data for kinesin-1 monomer showed that the NL in the forward orientation clashes severely with a nucleotide-binding motif (a P-loop subdomain) in the orientation of the $\phi$ state, implying the P-loop subdomain in the orientation of the ATP-like state.[52] Thus, the rate of ATP transition to ADP of the monomer with its NL in the forward orientation would be much higher than that with its NL not in the forward NL orientation, consistent with the biochemical data showing that deleting the NL in the kinesin-1 or kinesin-3 monomer significantly decreases the ATPase rate but has no effect on the ADP-release rate.[52,53] The rate constants of the ATPase activity are independent of the force on the NL. This agrees with the experimental results that the ATPase rate is independent of the NL length for the kinesin-1 dimer because varying the length greatly changes the force on the NLs[54] and the ATPase rate of the kinesin-1 monomer is similar to that of the dimer[55–57] because for the dimer a large force is present on the NLs whereas for the monomer no force is present.

In the assembly of two coupled monomers, each monomer is connected to the cargo by an appended single α-helix domain or stalk after the NL of the monomer, as in the experiments of Schimert *et al.*[34] Here, we simply consider that the distance between the two connecting points of the stalk on the cargo is equal to $md$, where $m \geq 2$ is an integer and $d = 8$ nm is the repeat period of tubulins on a MT filament. We focus on saturating ATP and use ATP to represent both ATP and ADP Pi. We suppose that the potential of a monomer interacting with a tubulin has a symmetric form along the MT filament. We take kinesin-1 as an example to illustrate the mechanochemical pathway of the two coupled monomers.

### 2.1. Pathway for two coupled monomers having a short stalk

In this section, we consider the stalk having a short length $L_S <$ 5 nm, as used in the experiments of Schimert *et al.*[34] Since $L_S <$ 5 nm is short, it is approximately considered that the stalk is not stretchable and bendable.

We start with the two monomers in the ATP state binding strongly to MT (Fig. 1a), where the two monomers can either be in a state having its NL docking in the forward orientation (lower panel), which is associated with a large conformational change relative to that in the ADP or $\phi$ state, or driven by the backward load in a state with its undocked NL in the backward orientation (upper panel), which is associated with no large conformational change. Note that the short stalk induces the NLs of the two monomers to dock and undock concertedly. The two states are in dynamic equilibrium, with rapid transitions between them.

In Fig. 1a, the ATP transition to ADP can occur independently in both monomers. Consider, *e.g.*, the ATP transition to ADP in the rear monomer. The rear monomer can detach from the local tubulin II due to the very small affinity $E_{w1}$. With probability $P_{E1}$, the detached monomer can diffuse forward and bind rapidly to tubulin III with affinity $E_{w2}$ by stretching its undocked NL to a length of about 4 nm (Fig. 1b) (note that the transition from the state in the lower panel of Fig. 1a to that in

Fig. 1b can cause little change in the position of the cargo). This transition of the rear monomer from the state in the lower panel of Fig. 1a to that in Fig. 1b is similar to the case for the dimer when one ATP-head is bound fixedly to MT and the other detached ADP-head diffuses from the intermediate position to the front adjacent tubulin by stretching the two NLs to a total length of $d = 8$ nm (see ESI text and Fig. S1†). Since the short total length of the stalk and NL keeps the detached ADP-monomer close to MT, the time (<1 μs) for the detached monomer to diffuse to the adjacent tubulin is much shorter than time $t_r$ (on the order of 10 μs)[58] and thus it is approximated that the detached monomer cannot rebind to the previous tubulin II. With probability $1 - P_{E1}$, the detached monomer can also diffuse backward and bind rapidly to tubulin I with affinity $E_{w2}$ (Fig. 1f) (note that the transition from the state in the upper panel of Fig. 1a to that in Fig. 1f can cause little change in the position of the cargo). Alternatively and more probably, after the ATP transition to ADP in the rear monomer, by overcoming the very small affinity $E_{w1}$ the monomer can (with probability $P_{E1}$) diffuse rapidly forward to front tubulin III and (with probability $1 - P_{E1}$) diffuse rapidly backward to rear tubulin I without detaching from MT. Since the affinity of tubulin III or I to the ADP-monomer, $E_{w2}$, is much larger than $E_{w1}$, after reaching tubulin III or I the ADP-monomer can stay there. (Note that this diffusion mechanism of the monomer from the local tubulin to the adjacent tubulin is similar to that for the motion of the kinesin-14 motor[59,60]).

In Fig. 1b, after ADP release from the rear monomer, ATP binds instantly (Fig. 1c). However, the large conformational change and NL docking of the rear monomer is inhibited, because the NL docking would induce a large forward movement of the cargo, requiring the further large stretching of the NL of the front monomer, which is impossible. As shown in Fig. 1f, after ADP release from the rear monomer, ATP binds instantly (Fig. 1g).

In Fig. 1c, the ATP transition to ADP in both monomers can occur independently, but with the front monomer with the NL in the forward orientation having a much higher rate of ATP transition to ADP than the rear monomer with the NL not in the forward orientation. Firstly, consider the ATP transition to ADP in the front monomer. The monomer cannot move backward and bind to tubulin I′, because further large stretching of the NL of the rear monomer is impossible. Thus, the monomer can only move forward and bind to tubulin III′ (Fig. 1d). Then, ADP release and ATP binding occur (Fig. 1e), with the system becoming the same as that in Fig. 1a (upper panel) except that in Fig. 1e the cargo moves a forward step of size $d$. Secondly, consider the ATP transition to ADP in the rear monomer in Fig. 1c. The monomer can only move backward and bind to tubulin II. After ADP release and ATP binding, the system returns to Fig. 1a (lower panel).

In Fig. 1g, the ATP transition to ADP in both monomers can occur independently. Firstly, consider the ATP transition to ADP in the front monomer. The monomer can only move backward and bind to tubulin I' (Fig. 1h). Then, ADP release and ATP binding occur (Fig. 1i), with the system becoming the same as that in Fig. 1a (lower panel) except that in Fig. 1i the cargo moves a backward step. Secondly, consider the ATP transition to ADP in the rear monomer. The monomer can only move forward and bind to tubulin II. After ADP release and ATP binding, the system returns to Fig. 1a (upper panel).

Similarly, in Fig. 1a for the case of the ATP transition to ADP occurring in the front monomer we have similar transitions (not shown) to those described above for the case of the ATP transition to ADP occurring in the rear monomer.

### 2.2. Pathway for two coupled monomers having a long stalk

In this section, we consider the stalk having a long length, as usually done in prior experimental and theoretical studies.[13–34] Since the stalk is long, it can be stretched or bent elastically. If after the ATP transition to ADP in one monomer it detaches from MT due to the small affinity $E_{w1}$, the detached monomer will fluctuate in a large range due to the long stalk and thus rebind to the MT with a slow rate of about 5 $s^{-1}$, as prior experimental data showed.[61] During the relatively long period before the rebinding of the detached monomer to MT, the ATP transition to ADP in another monomer can occur with a high rate of about 100 $s^{-1}$.[55] The ensuing detachment of the latter monomer results in the detachment of the cargo from MT and thus the cargo cannot move processively along the MT. Consequently, here we only consider the more probable case that after the ATP transition to ADP in one monomer it can diffuse from the local tubulin to the adjacent tubulin by overcoming $E_{w1}$ without detaching from MT. After reaching the adjacent tubulin, the monomer can stay there due to the larger affinity $E_{w2}$.

We start with the two monomers in the ATP state binding strongly to MT, where the NL of each monomer are mainly in the docked form (Fig. 2a) or occasionally in the undocked form (not shown). The ATP transition to ADP in both monomers can occur. Consider, *e.g.*, the ATP transition to ADP in the front monomer. The front monomer can either (with probability $P_{E0}$) diffuse forward to the front tubulin III′ or (with probability $1 - P_{E0}$) diffuse backward to the rear tubulin I′ by overcoming the very small affinity $E_{w1}$. Note that due to the long stalk the backward diffusion of the front ADP-monomer to tubulin I′ does not necessarily result in the NL undocking of the rear ATP-monomer. After reaching tubulin III′ or I′ the ADP-monomer can stay there due to the larger affinity $E_{w2}$ (Fig. 2b or e). After ADP release from the front monomer, ATP binding and NL docking occur (Fig. 2c or f).

In Fig. 2c and f, the ATP transition to ADP in both monomers can occur. Firstly, consider the ATP transition to ADP in the front monomer in Fig. 2c or f. By overcoming $E_{w1}$, the front monomer diffuses to the adjacent tubulin II′, where no internal force is present on the two monomers (for simplicity, we do not consider the front monomer diffusing to the other adjacent tubulins because this will induce an increase in the internal force). After reaching tubulin II' the ADP-monomer stays there due to the larger affinity $E_{w2}$ and then ADP is released, followed by ATP binding and NL docking (Fig. 2a). Secondly, consider the ATP transition to ADP in the rear monomer in Fig. 2c. By overcoming $E_{w1}$, the rear monomer diffuses to the adjacent

tubulin III, where no internal force is present on the two monomers (for simplicity, we do not consider the rear monomer diffusing to the adjacent tubulin I because this will induce an increase in the internal force). After reaching tubulin III the ADP-monomer stays there due to the larger affinity $E_{w2}$ and then ADP is released, followed by ATP binding and NL docking (Fig. 2d). The state of the system in Fig. 2d is the same as that in Fig. 2a except that in Fig. 2d the cargo moves a forward step. Thirdly, consider the ATP transition to ADP in the rear monomer in Fig. 2f. By overcoming $E_{w1}$, the rear monomer diffuses to the adjacent tubulin I, where no internal force is present on the two monomers (for simplicity, we do not consider the rear monomer diffusing to the adjacent tubulin III because this will induce an increase in the internal force). After reaching tubulin I the ADP-monomer stays there due to the larger affinity $E_{w2}$ and then ADP is released, followed by ATP binding and NL docking (Fig. 2g). The state of the system in Fig. 2g is the same as that in Fig. 2a except that in Fig. 2g the cargo moves a backward step.

Similarly, in Fig. 2a for the case of the ATP transition to ADP occurring in the rear monomer we have similar transitions to those described above for the case of the ATP transition to ADP occurring in the front monomer (not shown).

# 3. Results and discussion

## 3.1. Dynamics of the single kinesin-1 dimer

The dynamics of the single dimer is studied on the basis of the mechanochemical pathway described in ESI text and Fig. S1.†

Consider a cargo connecting to the stalk of the dimer in the optical trapping experiment. $\kappa$ denotes the effective elastic constant of the trap and the stalk. Since in the trapping experiment the elastic constant of the trap $\kappa_{trap}$, usually has a very small value (<0.05 pN nm$^{-1}$),[9,10,62,63] $\kappa = \kappa_{trap}\kappa_{stalk}/(\kappa_{trap} + \kappa_{stalk})$ is very small, where $\kappa_{stalk}$ is the elastic constant of the stalk. As derived before,[64] for a very small $\kappa$ the effective probability $P_{E2}$ for the dimer (defined in Fig. S1†) approximately has the form

$$P_{E2} = \frac{\exp(\beta E_0)\exp(-\beta\lambda Fd)}{\exp(\beta E_0)\exp(-\beta\lambda Fd) + 1}, \quad (1)$$

where $E_0$ is the energy change associated with the NL docking and the large conformational change of the monomer in the ATP state relative to that in the $\phi$ or ADP state, $\beta^{-1} = k_BT$, with $k_B$ being the Boltzmann constant and $T$ the absolute temperature, $F$ is the backward load on the cargo, with $Fd$ being the increase in the external energy of the motor-cargo system for a forward step or the work done by the motor per forward step, and $\lambda$ ($\leq$1) is the energy-splitting factor. Since the effect of $F$ on $P_{E2}$ is through the force on the NLs of the two heads and is irrelevant to the stalk, it is expected that $P_{E2}$ is independent of the stalk length under the condition of the very small elastic constant of the trap in the optical trapping experiment.

$k^{(+)}$ and $k^{(-)}$ denote the rate of the ATP transition to ADP of the monomer with a forward NL orientation and that without a forward NL orientation, respectively. Since ADP release from the MT-bound ADP-monomer is a non-rate-limiting step of the ATPase activity,[55] for simplicity, here we assume that the rate of ADP release from the MT-bound ADP-monomer, $k_D$, is much larger than $k^{(+)}$. Thus, the velocity, $v$, and stepping ratio, $r$, of the dimer can be approximately written as[41,64]

$$v = [P_{E2}k^{(+)} - (1 - P_{E2})k^{(-)}]d, \quad (2)$$

$$r = \frac{P_{E2}k^{(+)}}{(1 - P_{E2})k^{(-)}}. \quad (3)$$

Since $k^{(+)}$ and $k^{(-)}$ depend only on the NL orientation, they are independent of the stalk length. As mentioned just above, $P_{E2}$ is also independent of the stalk length under the condition of the very small elastic constant of the trap in the optical trapping experiment. Thus, eqn (2) and (3) are independent of the stalk length.

By adjusting values of parameters, $k^{(+)}$, $k^{(-)}$, $E_0$ and $\lambda$ (Table 1), eqn (1)–(3) fit the experimental data well on velocity $v$ and stepping ratio $r$ *versus* load $F$ measured by Nishiyama *et al.*[9] at saturating (1 mM) ATP (Fig. 3). The rate of the ATP transition to ADP for the trailing head with the forward NL orientation, $k^{(+)} = 128$ s$^{-1}$, is close to the biochemical value for the truncated monomer whose NL after ATP binding docks rapidly in the forward orientation.[55] The rate of the ATP transition to ADP for the leading head with the backward NL orientation, $k^{(-)} = 2$ s$^{-1}$, is 64-fold smaller than $k^{(+)}$, which is consistent with the biochemical data showing that deleting the NL decreases the rate of the ATP transition to ADP by about 60-fold.[52] The total rate of the ATP transition to ADP, $k^{(+)} + k^{(-)} = 130$ s$^{-1}$, for the dimer, is close to that, $k^{(+)} = 128$ s$^{-1}$, for the monomer, which is consistent with the biochemical data showing that rate of the ATP transition to ADP for the dimer is similar to that for the monomer.[55–57] The small value of $E_0 = 2.2k_BT$ agrees with the available experimental data indicating that the energy change associated with the NL docking is <1$k_BT$,[65] and the all-atom molecular dynamics simulation data indicating that the energy change associated with the large conformational change of the kinesin monomer induced by ATP binding is only a few $k_BT$.[66]

## 3.2. Dynamics of two coupled kinesin-1 monomers having a short stalk

In the assembly of two coupled monomers, each monomer is connected to the cargo by an appended single α-helix domain or

Table 1 Parameter values for kinesin-1

| Parameter | Description | Value |
|---|---|---|
| $k^{(+)}$ | Rate of the ATP transition to ADP in a monomer with its NL in the forward orientation | 128 s$^{-1}$ |
| $k^{(-)}$ | Rate of the ATP transition to ADP in a monomer with its NL not in the forward orientation | 2 s$^{-1}$ |
| $E_0$ | Energy change of NL docking and large conformational change of the ATP-monomer | 2.2$k_BT$ |
| $\lambda$ | Energy-splitting factor | 0.425 |

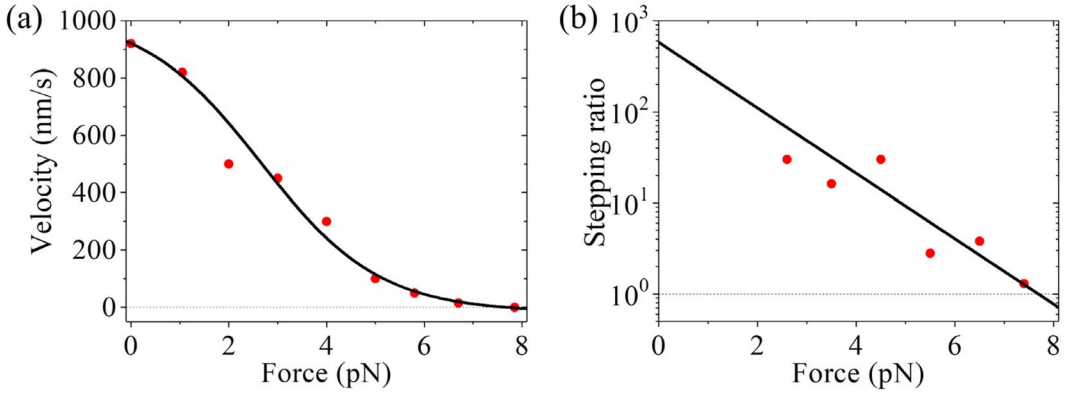


Fig. 3 Results for the dynamics of the single kinesin-1 dimer. Solid lines represent theoretical results. Symbols are experimental data at saturating (1 mM) ATP taken from Nishiyama *et al.*[9] (a) Velocity *versus* load. (b) Stepping ratio *versus* load.

stalk after the NL of the monomer, as in the experiments of Schimert *et al.*[34] In this section, we study the dynamics of cargo transport by the two coupled monomers with the stalk having a short length $L_S < 5$ nm. The mechanochemical pathway is shown in Fig. 1.

As shown in Fig. 1, the state of the system in the upper panel and that in the lower panel of Fig. 1a are in dynamic equilibrium, with the state in the lower panel having lower energy by about $\Delta E = 2E_0 - Fd$ relative to that in the upper panel under the backward load $F$ on the cargo. Thus, the probability of the system in the state of the lower panel is

$$P_{\mathrm{NL}} = \frac{\exp[\beta(2E_0 - Fd)]}{\exp[\beta(2E_0 - Fd)] + 1}. \tag{4}$$

In the state of the lower panel, the rate of the ATP transition to ADP in any monomer with the NL in the forward orientation is $k^{(+)}$. In the state of the upper panel, the rate of the ATP transition to ADP in any monomer with the NL in the backward orientation is $k^{(-)}$. Thus, the overall rate of the ATP transition to ADP in one monomer in Fig. 1a is

$$k_{\mathrm{a}} = P_{\mathrm{NL}}k^{(+)} + (1 - P_{\mathrm{NL}})k^{(-)}. \tag{5}$$

After the ATP transition to ADP in one monomer (*e.g.*, the rear monomer) in Fig. 1a, the effective probability $P_{\mathrm{E1}}$ for the system to transition to Fig. 1b can be derived as follows, similar to that done before for the case of the dimer.[64] It is noted that the internal energy of the system in the state in Fig. 1f is higher than that in Fig. 1b by $E_0$. For the simple unloaded case, no external energy change is present for the transition from Fig. 1a to b and that from Fig. 1a to f, and thus considering the symmetrical potential of the monomer interacting with tubulin, the rate of the transition from Fig. 1a to b and that from Fig. 1a to f can be written as $k_{\mathrm{Front}} = C$ and $k_{\mathrm{Rear}} = C\exp(-\beta_{\mathrm{E0}})$, respectively, where $C$ is a constant. For the loaded case, we use $\varepsilon_0$ to denote the external energy of the system in the state in Fig. 1a, $\varepsilon_1$ to denote the external energy in the state in Fig. 1b and $\varepsilon_{-1}$ to denote the external energy in the state in Fig. 1f at one moment. Of the external energy change $\varepsilon_1 - \varepsilon_0$ the fraction perturbing the transition from Fig. 1a to b is $\lambda$. Similarly, of the external energy change $\varepsilon_{-1} - \varepsilon_0$ the fraction perturbing the transition from Fig. 1a to f is also $\lambda$. Thus, the transition rate from Fig. 1a to b and that from Fig. 1a to f can be written as $k_{\mathrm{Front}} = C\exp[-\beta\lambda(\varepsilon_1 - \varepsilon_0)]$ and $k_{\mathrm{Rear}} = C\exp(-\beta_{\mathrm{E0}})\exp[-\beta\lambda(\varepsilon_{-1} - \varepsilon_0)]$, respectively. The probability $P_{\mathrm{E1}}$ can be calculated with $P_{\mathrm{E1}} = k_{\mathrm{Front}}/(k_{\mathrm{Front}} + k_{\mathrm{Rear}})$, which is written as

$$P_{\mathrm{E1}} = \frac{\exp(\beta E_0)\exp[-\beta\lambda(\varepsilon_1 - \varepsilon_{-1})]}{\exp(\beta E_0)\exp[-\beta\lambda(\varepsilon_1 - \varepsilon_{-1})] + 1}. \tag{6}$$

As in the above section, consider that in the optical trapping experiment the elastic constant of the trap $k_{\mathrm{trap}}$, is very small (<0.05 pN nm$^{-1}$).[9,10,62,63] Then, it is noted that whether the ATP transition to ADP occurs in the rear monomer in the lower panel or in the upper panel of Fig. 1a, the external elastic energy for the transition from Fig. 1a to b is increased approximately by $Fd$ relative to that for the transition from Fig. 1a to f, giving $\varepsilon_1 - \varepsilon_{-1} = Fd$. Thus, eqn (6) can be rewritten as

$$P_{\mathrm{E1}} = \frac{\exp(\beta E_0)\exp(-\beta\lambda Fd)}{\exp(\beta E_0)\exp(-\beta\lambda Fd) + 1}. \tag{7}$$

Since the two states in the upper and lower panels of Fig. 1a can transition rapidly from each other and $k_{\mathrm{D}}$ is much larger than $k^{(+)}$, it is noted that after the ATP transition to ADP occurs in the rear monomer in Fig. 1a, the rate of the transition from Fig. 1a to e, equivalent to the rate of a forward step of the cargo, is approximately given by $k_{\mathrm{Fwd}} = P_{\mathrm{E1}}k_{\mathrm{a}}k^{(+)}/(P_{\mathrm{E1}}k_{\mathrm{a}} + k^{(+)})$. In the same way, the rate of the transition from Fig. 1a to i, equivalent to the rate of a backward step of the cargo, is approximately given by $k_{\mathrm{Bwd}} = (1 - P_{\mathrm{E1}})k_{\mathrm{a}}k^{(-)}/[(1 - P_{\mathrm{E1}})k_{\mathrm{a}} + k^{(-)}]$. Similarly, after the ATP transition to ADP occurs in the front monomer in Fig. 1a, we have the same forward and backward stepping rates $k_{\mathrm{Fwd}}$ and $k_{\mathrm{Bwd}}$ for the cargo. Since in Fig. 1a the ATP transition to ADP can occur in both monomers with the same rate, the cargo velocity is approximately $v = 2(k_{\mathrm{Fwd}} - k_{\mathrm{Bwd}})d$, which is rewritten as

$$v = 2\left[\frac{P_{\mathrm{E1}}k_{\mathrm{a}}k^{(+)}}{P_{\mathrm{E1}}k_{\mathrm{a}} + k^{(+)}} - \frac{(1 - P_{\mathrm{E1}})k_{\mathrm{a}}k^{(-)}}{(1 - P_{\mathrm{E1}})k_{\mathrm{a}} + k^{(-)}}\right]d. \tag{8}$$

The forward to backward stepping ratio is approximately $r = k_{Fwd}/k_{Bwd}$, which is written as

$$r = \frac{P_{E1}k^{(+)}\left[(1-P_{E1})k_a + k^{(-)}\right]}{(1-P_{E1})k^{(-)}\left(P_{E1}k_a + k^{(+)}\right)}. \quad (9)$$

Using eqn (4)–(9) and with parameter values given in Table 1, the theoretical results of velocity $v$ and stepping ratio $r$ *versus* $F$ are shown in Fig. 4. By comparing Fig. 4a with Fig. 3a it is interesting to see that under a near-zero load, the velocity for the two coupled monomers is similar to that for the single dimer. However, as the backward load increases, for the two coupled monomers the velocity decreases quicker than for the single dimer. The stall force for the two coupled monomers is about 4 pN and that for the single dimer is about 7.7 pN, with the latter being about 2-fold larger than the former. This gives an explanation of why in cells cargo transport is designed to be realized by kinesin dimers rather than by multiple monomers with a short stalk. The above theoretical results are consistent with the experimental evidence from Schimert *et al.*[34] showing that multiple coupled monomers can drive cargo to move toward the MT plus end with a high velocity under a low external load but with a small driving force. By comparing Fig. 4b with Fig. 3b it is seen that the unloaded stepping ratio for the two coupled monomers is about 17 times smaller than that for the single dimer, further explaining why in cells cargo transport is designed to be realized by kinesin dimers. Interestingly, it is seen that while for the single dimer the stepping ratio decreases exponentially with the increase in the load (Fig. 3b), for the two coupled monomers the stepping ratio *versus* the load does not follow the exponential form (Fig. 4b).

To understand the underlying mechanism of the two coupled monomers having an evidently smaller stall force than the single dimer, in Fig. 5 (black solid lines) we show the results of $v$ and $r$ *versus* $F$ with $P_{NL} = 1$, namely with the two ATP-monomers in Fig. 1a always being in the state having the docked NL (the lower panel). For comparison, in Fig. 5 we also reshow the results given in Fig. 3 (red dashed lines) and those given in Fig. 4 (blue dashed-dotted lines). It is seen that $v$ and $r$ under no load with $P_{NL} = 1$ for the two coupled monomers are nearly equal to those with $P_{NL} \neq 1$. However, the stall force with $P_{NL} = 1$ for the two coupled monomers becomes nearly equal to that for the single dimer. Thus, the large probability of the ATP-monomers in Fig. 1a to be in the state with an undocked NL (the upper panel) under the backward load leads to the two coupled monomers having an evidently smaller stall force than the single dimer. The differences in the dynamics between the two coupled monomers and the single dimer can be noted intuitively from the pathways shown in Fig. 1 and S1,† as stated as follows.

For the dimer (Fig. S1†), which is predominantly in the two-heads-bound (2HB) state during its mechanochemical cycle,[67,68] the relative position of the two heads in the 2HB state ensures that the NLs of the trailing and leading heads are always in the forward and backward orientations, respectively, under any backward load. This thus gives higher and lower rates of ATP transition to ADP in the trailing and leading heads, respectively, because the orientation of the NL dictates the rate of the ATP transition to ADP of the head. On the other hand, the transition of ATP to ADP in the trailing head can lead to either a forward step or a futile mechanochemical cycle while the transition of ATP to ADP in the leading head can lead to either a backward step or a futile mechanochemical cycle (Fig. S1†). Hence, the dimer can have a high stepping ratio and thus a large stall force. By contrast, for the two coupled monomers (Fig. 1), the ATP-monomers in Fig. 1a can be driven by the backward load to be in the state with the NL not in the forward orientation (the upper panel). This results in a large decrease in the rate of ATP transition to ADP of the two monomers as shown in Fig. 1a and thus a large decrease in the forward stepping rate under the backward load, providing a small stall force. This advantage of the dimer over the two coupled monomers, namely the NL of the trailing head always being in the forward orientation under any backward load for the dimer and the NL not always being in the forward orientation for the two coupled monomers, provides an explanation of why the native kinesin is designed to be in the dimeric form.

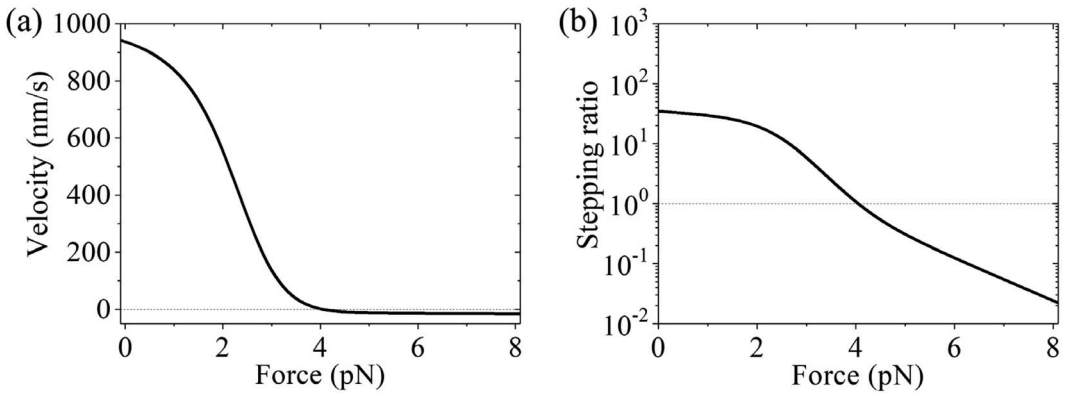


Fig. 4 Results for the dynamics of cargo transport by two coupled kinesin-1 monomers with a short stalk. (a) Velocity *versus* load. (b) Stepping ratio *versus* load.

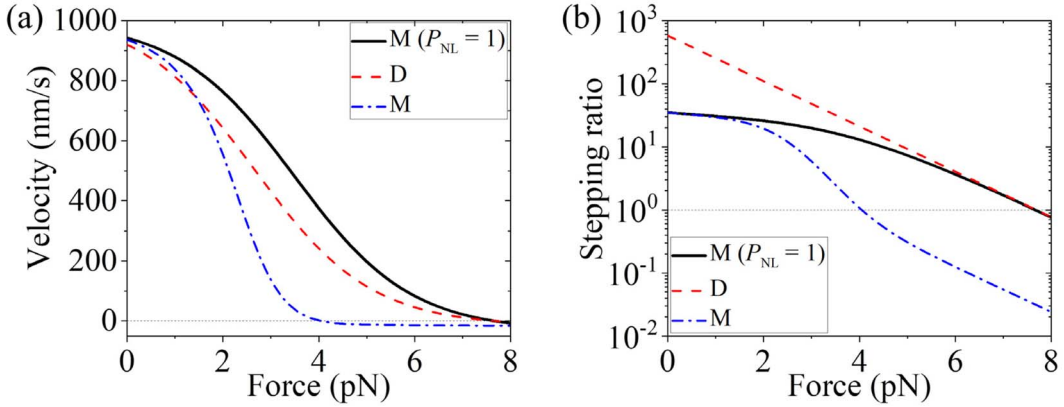


Fig. 5 Results for the dynamics of cargo transport by two coupled kinesin-1 monomers with a short stalk for the case of $P_{NL} = 1$ (black solid lines). For comparison, the results shown in Fig. 3 (red dashed lines) and in Fig. 4 (blue dashed-dotted lines) are reshown. $M(P_{NL} = 1)$: two coupled monomers with a force-independent NL orientation setting $P_{NL} = 1$, *D*: one dimer, and *M*: two coupled monomers with a force-dependent NL orientation. (a) Velocity *versus* load. (b) Stepping ratio *versus* load.

### 3.3. Dynamics of two coupled kinesin-1 monomers having a long stalk

In this section, we study the dynamics of cargo transport by two coupled monomers with a long wild-type stalk. The mechano-chemical pathway is shown in Fig. 2. As prior experimental results indicated, the elastic constant of the long stalk of the kinesin, $\kappa_{stalk}$, is about 0.3 pN nm$^{-1}$.[69,70] Thus, the elastic energy for one monomer in either Fig. 2c or f, which arises from stretching of its stalk, is increased approximately by $E_{elas} = \kappa_{stalk}(d/2)^2/2 = 0.58k_BT$ relative to that in Fig. 2a. This value of $E_{elas}$ is evidently smaller than $E_0 = 2.2k_BT$, implying that after ATP binding to the front monomer bound to tubulin III′ (Fig. 2c) or I′ (Fig. 2f) its NL docking can occur easily.

Similar to eqn (4) and (5), the overall rate of ATP transition to ADP in one monomer in Fig. 2a has the form

$$k_a = P_{NL0}k^{(+)} + (1 - P_{NL0})k^{(-)}, \tag{10}$$

$$P_{NL0} = \frac{\exp[\beta(E_0 - Fd/4)]}{\exp[\beta(E_0 - Fd/4)] + 1}, \tag{11}$$

where due to the long stalk one monomer can be in the state with either a docked or undocked NL independent of the other monomer. This is contrary to the case of the short stalk shown in Fig. 1a, where the short stalk induces the NLs of the two monomers to dock and undock concertedly. Similar to eqn (10) and (11), the overall rate of ATP transition to ADP in the rear monomer in Fig. 2c and that in the front monomer in Fig. 2f, whose stalks are elastically stretched in the forward direction, have the form

$$k_a^{(+)} = P_{NL0}^{(+)}k^{(+)} + (1 - P_{NL0}^{(+)})k^{(-)}, \tag{12}$$

$$P_{NL0}^{(+)} = \frac{\exp[\beta(E_0 + E_{elas} - Fd/4)]}{\exp[\beta(E_0 + E_{elas} - Fd/4)] + 1}, \tag{13}$$

where $E_{elas} = 0.58k_BT$ (see above). Similarly, the overall rate of ATP transition to ADP in the front monomer in Fig. 2c and that in the rear monomer in Fig. 2f, whose stalks are elastically stretched in the backward d direction, have the form

$$k_a^{(-)} = P_{NL0}^{(-)}k^{(+)} + (1 - P_{NL0}^{(-)})k^{(-)}, \tag{14}$$

$$P_{NL0}^{(-)} = \frac{\exp[\beta(E_0 - E_{elas} - Fd/4)]}{\exp[\beta(E_0 - E_{elas}) - Fd/4] + 1}. \tag{15}$$

For the approximation of $k_D \gg k^{(+)}$, from Fig. 2 we use the following equations for the velocity and stepping ratio of the cargo

$$v = 2\left[\frac{P_{E0}k_a k_a^{(+)}}{P_{E0}k_a + k_a^{(+)}} - \frac{(1 - P_{E0})k_a k_a^{(-)}}{(1 - P_{E0})k_a + k_a^{(-)}}\right]d, \tag{16}$$

$$r = \frac{P_{E0}k_a^{(+)}\left[(1 - P_{E0})k_a + k_a^{(-)}\right]}{(1 - P_{E0})k_a^{(-)}\left(P_{E0}k_a + k_a^{(+)}\right)}, \tag{17}$$

where $P_{E0}$ is the effective probability (defined in Fig. 2), which can be derived as follows. It is noted that in Fig. 2e the elastic energy for the system, which arises from the stretching of the two stalks, is increased by about $2E_{elas}$ relative to that in Fig. 2a. As shown in Fig. 2e the energy change for the NL docking of the rear ATP-monomer is decreased by about $E_{elas}$ relative to that in Fig. 2a. For the very small elastic constant of the trap, $\kappa_{trap}$, the external elastic energy of the system for the transition from Fig. 2a to e, which arises from the external load, is decreased by about $Fd/2$ relative to that for the transition from Fig. 2a to a. Thus, compared to Fig. 2a, the total energy change in Fig. 2e is increased by about $E_{elas} - Fd/2$ relative to that in Fig. 2b. Hence, similar to the derivation of eqn (7), $P_{E0}$ can be derived as

$$P_{E0} = \frac{\exp[\beta\lambda(E_{elas} - Fd/2)]}{\exp[\beta\lambda(E_{elas} - Fd/2)] + 1}. \tag{18}$$

Using eqn (10)–(18) and with parameter values given in Table 1, the theoretical results of $v$ and $r$ *versus* $F$ are shown in Fig. 6. By comparing Fig. 6a with Fig. 4a it is interesting to see that the unloaded velocity for the two coupled monomers with a long stalk is about 124 nm s$^{-1}$, which is reduced by about 7.6 times

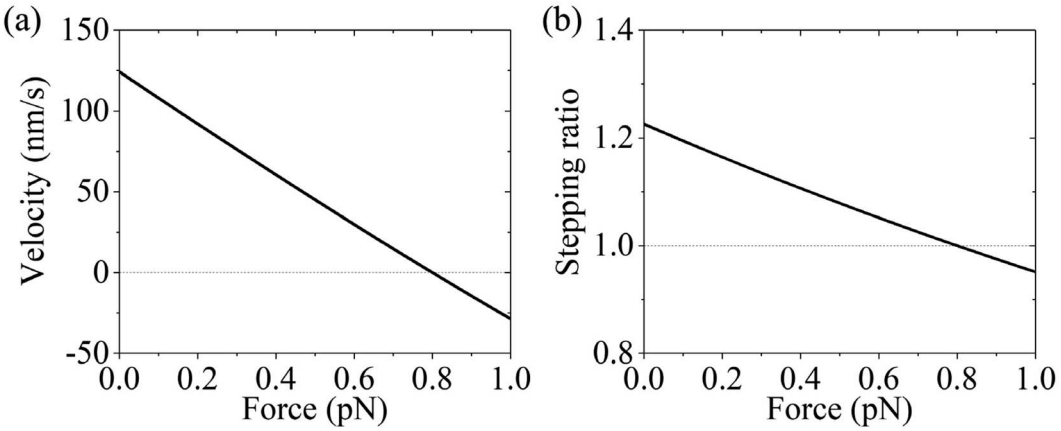


Fig. 6 Results for the dynamics of cargo transport by two coupled kinesin-1 monomers with a long stalk. (a) Velocity *versus* load. (b) Stepping ratio *versus* load.

relative to that for the two coupled monomers with a short stalk (about 941 nm $s^{-1}$). Moreover, the stall force for the two coupled monomers with a long stalk is only about 0.8 pN, which is reduced by about 5 times relative to that for the two coupled monomers with a short stalk (about 4 pN). These theoretical results are consistent with the experimental evidence from Schimert *et al.*[34] From Fig. 6b it is seen that under no load the stepping ratio is about 1.2, which is only slightly larger than 1. By contrast, from Fig. 4b it is seen that under no load the stepping ratio is about 34.8, which is much larger than 1.

### 3.4. Dynamics of two coupled kinesin-2 KIF3A monomers

In Section 3.2, it is shown that the decrease in the stall force for the two coupled kinesin-1 monomers with a short stalk relative to that for the single kinesin-1 dimer is due to two reasons. One is that the ATP-monomers in Fig. 1a can be driven by the backward load to be in the state with the NL in the backward orientation. The other one is that the monomer with the NL in the backward orientation has a much smaller rate of ATP transition to ADP than that with the NL in the forward orientation. Thus, if the rate of ATP transition to ADP in the monomer with the backward NL has a small difference from or is similar to that with the forward NL, the stall force for the two coupled monomers with a short stalk would be slightly smaller than or similar to that for the single dimer.

In the pathway for the dimer (Fig. S1†), the forward stepping rate of the dimer is induced by the transition of ATP to ADP in the trailing head while the backward stepping of the dimer is induced by the transition of ATP to ADP in the leading head, with the forward and backward stepping rates being $P_{E2}k^{(+)}$ and $(1 - P_{E2})k^{(-)}$, respectively. This implies that for a type of kinesin dimer having a large unloaded backstepping probability the rate of ATP transition to ADP in its head with the backward NL, $k^{(-)}$, would have a smaller difference from that with the forward NL, $k^{(+)}$, than for another type having a small unloaded backstepping probability if the two types have similar $P_{E2}$ or $E_0$. Thus, it is expected that for a type of kinesin dimer having a large unloaded backstepping probability, the two coupled monomers of this type with a short stalk would have a stall force that is slightly smaller than or similar to that for a kinesin dimer of the same type. Prior experimental studies showed that a kinesin-2 KIF3AA, KIF3BB or KIF3AB dimer has an evidently larger backstepping probability than the kinesin-1 dimer.[71,72] Thus, to verify the aforementioned expectation, in this section we study the dynamics of the two coupled kinesin-2 KIF3A monomers compared with that of the single KIF3AA, KIF3BB or KIF3AB dimer.

Firstly, we consider KIF3AA, KIF3BB and KIF3AB dimers. For simplicity, we suppose that for this type of kinesin the NL orientation has no effect on the rate of ATP transition to ADP of the head. This means that $k^{(+)} = k^{(-)}$ and thus only three parameters $k^{(+)}$, $E_0$ and $\lambda$ are adjustable in eqn (1)–(3). By taking $k^{(+)} = 64\ s^{-1}$, $E_0 = 3.5k_BT$ and $\lambda = 0.23$, the theoretical results for the load dependence of velocity are consistent with the available experimental data (Fig. 7a, black line). The theoretical results for the backstepping probability $P_{back} = 1/(r + 1)$ are shown in Fig. 7b (black line), where $r$ is the stepping ratio defined above. For comparison, the available experimental data are also shown in Fig. 7b (symbols). Since the three experimental data in Fig. 7b are measured by different research groups and using different methods, the data at the backward load $F = 1$ pN and $F = 4$ pN are smaller than that at $F = 0$, which is contrary to the fact that the backstepping probability under no load should be smaller than those under non-zero backward loads. Nevertheless, from Fig. 7b it is seen that the theoretical results are on the same order as the experimental data. By comparing Fig. 7a for the KIF3AA, KIF3BB and KIF3AB dimers with Fig. 3a for the kinesin-1 dimer, it is noted that although the unloaded velocity for the former (about 485 nm $s^{-1}$) is about 2-fold smaller than that for the latter (about 920 nm $s^{-1}$) the stall force for the former (about 7.8 pN) is close to that for the latter (about 7.7 pN).

Secondly, we consider the two coupled KIF3A monomers with a short stalk. With the above three parameter values and using eqn (4)–(9), the theoretical results of $v$ and $P_{back}$ *versus* $F$ are also shown in Fig. 7 (red lines). It is interesting to see that the theoretical results of $v$ *versus* $F$ for the two coupled

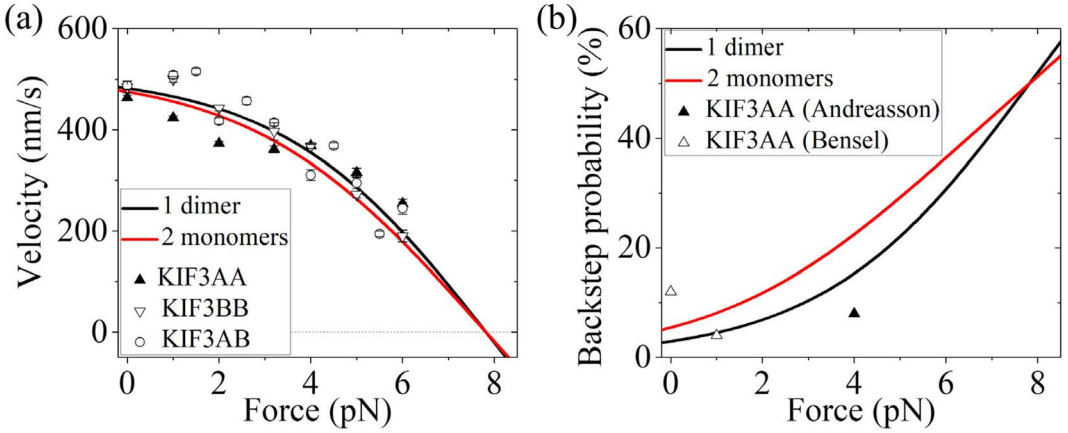


Fig. 7 Results for the dynamics of cargo transport by the single kinesin-2 KIF3AA, KIF3BB or KIF3AB dimer (black lines) and that by two coupled kinesin-2 KIF3A or KIF3B monomers with a short stalk (red lines). The parameter values are $k^{(+)} = k^{(-)} = 64\ s^{-1}$, $E_0 = 3.5k_BT$ and $\lambda = 0.23$. (a) Velocity *versus* load. Symbols are experimental data from Andreasson *et al.*[71] (b) Backstepping probability *versus* load. Filled symbol is the experimental value (at $F = 4$ pN) from Andreasson *et al.*[71] measured using the optical trapping method. Unfilled symbols are experimental data from Bensel *et al.*,[72] with the value at $F = 0$ measured using interferometric scattering (iSCAT) microscopy and that at $F = 1$ pN measured using the optical trapping method.

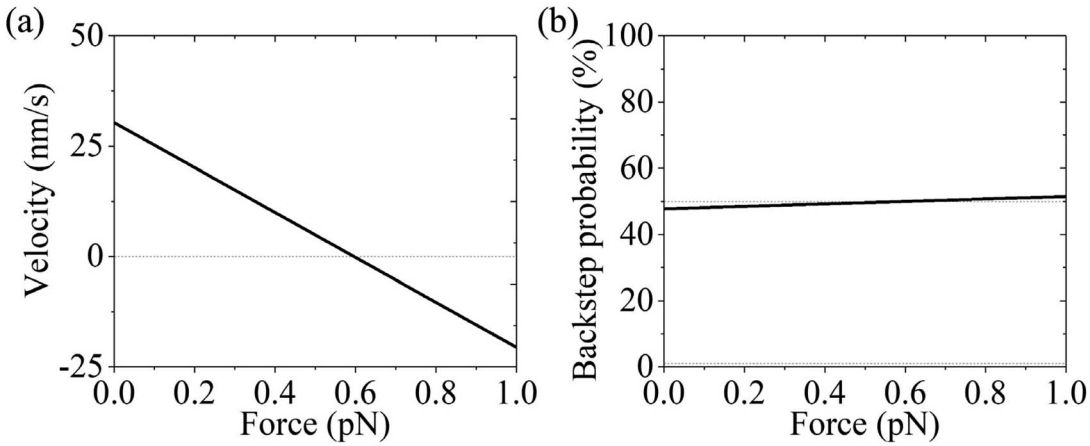


Fig. 8 Results for the dynamics of cargo transport by two coupled kinesin-2 KIF3A or KIF3B monomers with a long stalk. The parameter values are the same as those in Fig. 7. (a) Velocity *versus* load. (b) Backstepping probability *versus* load.

monomers are close to those for the single dimer, and more interestingly the stall force for the two coupled monomers is the same as that for the single dimer. These are in agreement with the experimental evidence from Schimert *et al.*[34] showing that multiple coupled KIF3A monomers with a short stalk can drive a high-load cargo, like multiple KIF3AB dimers.

Thirdly, we consider the two coupled KIF3A monomers with a long stalk. With the above three parameter values and using eqn (10)–(18), the theoretical results of $v$ and $P_{back}$ *versus* $F$ are shown in Fig. 8, with the unloaded velocity being only about 30 nm $s^{-1}$ and the stall force being only about 0.59 pN. By comparing Fig. 8a with Fig. 7a it is interesting to see that both the unloaded velocity and stall force for the two coupled monomers with a long stalk are much smaller than those with a short stalk. From Fig. 8b it is seen that under the load in the range of 0–1 pN the backstepping probabilities are close to 50%. As expected, the backstepping probability under no load in Fig. 8b is much larger than that in Fig. 7a.

Note that if we assume $k^{(+)} > k^{(-)}$, for example, taking $k^{(+)} = 64.5\ s^{-1}$, $k^{(-)} = 0.5k^{(+)}$, $E_0 = 2.9k_BT$ and $\lambda = 0.21$, the theoretical results for the load dependences of the velocity $v$ and backstepping probability $P_{back}$ for the single dimer can also be consistent with the available experimental data (Fig. S2,† black lines). With the above four values and using eqn (4)–(9), the theoretical values of $v$ and $P_{back}$ *versus* $F$ for the two coupled KIF3A monomers with a short stalk are also shown in Fig. S2† (red lines). It is seen that the unloaded velocity for the two coupled monomers is similar to that for the single dimer and the stall force for the two coupled monomers is only slightly smaller than that for the single dimer. These are also consistent with the experimental evidence from Schimert *et al.*[34]

Taken together, in this section together with Section 3.2 we consistently explain the puzzling experimental data showing that multiple kinesin-1 monomers, unlike the corresponding dimers, cannot drive high-load cargo, whereas multiple KIF3A monomers, like the corresponding dimer, can drive high-load cargo.[34] In addition, prior studies showed that for kinesin-3 KIF1A, the rate of ATP transition to ADP in its head with the NL not in the forward orientation is much smaller than that with the NL in the forward orientation,[53,73] like kinesin-1. Thus, it is expected that the dynamics of the two coupled KIF1A monomers relative to the single KIF1A dimer is similar to that of the two coupled kinesin-1 monomers relative to the single kinesin-1 dimer and is in contrast to that of the two coupled KIF3A monomers relative to the single KIF3AA or KIF3AB dimer. This is also consistent with the experimental evidence from Schimert *et al.*[34]

# 4. Concluding remarks

Based on the mechanochemical pathway of the kinesin dimer presented before, the mechanochemical pathway of the two coupled monomers is presented here. With the pathways, the dynamics of the two coupled monomers is studied theoretically and compared with that of the corresponding single dimer. It is shown that if the stalk, which connects the NL of the monomer and the cargo, has a short length $L_S$ (*e.g.*, $L_S < 5$ nm), the cargo transport by the two coupled monomers can be efficient with the unloaded velocity similar to that by the single dimer. By contrast, if $L_S$ is long, the cargo transport can be inefficient with a much smaller unloaded velocity and a much smaller stall force than those by the two monomers with a short $L_S$. Thus, it is deduced that cargo transport by the two coupled monomers depends significantly on the stalk length, with the unloaded velocity and stall force decreasing with the increase in the stalk length. By contrast, the dynamics of the dimer is irrelevant to the stalk length. These are consistent with the available experimental evidence.[34] Although the unloaded velocity for the two coupled kinesin-1 (or kinesin-3 KIF1A) monomers is similar to that for the corresponding single dimer, the stall force for the former is about 2-fold smaller than that for the latter. By contrast, both the unloaded velocity and stall force for the two coupled kinesin-2 KIF3A monomers are similar to those for the single KIF3AA, KIF3BB or KIF3AB dimer. The underlying mechanism of the two coupled kinesin-1 (or kinesin-3 KIF1A) monomers with a short stalk having an evidently smaller stall force than the corresponding single dimer and the two coupled kinesin-2 KIF3A monomers with a short stalk having a stall force similar to that of the corresponding single dimer is explored. Moreover, the predicted results on the load dependence of the stepping ratio of the two coupled monomers are also provided (Fig. 4b, 6b, 7b and 8b).

A predominant difference between cargo transport by the two coupled monomers (Fig. 1) and that by the single dimer (Fig. S1†) is that in the former the two monomers step in an inchworm manner while in the latter the two heads step in a hand-over-hand manner. The hand-over-hand stepping manner ensures that the NLs of the trailing and leading heads in the ATP state are always in the forward and backward orientations, respectively, under any backward load, resulting in a higher stall force for the kinesin-1 (or kinesin-3) dimer. By contrast, the inchworm stepping manner does not ensure that the NLs of the two monomers in the ATP state are always in the forward orientation, resulting in a smaller stall force for the two coupled kinesin-1 (or kinesin-3) monomers. This gives an explanation of why the kinesin dimer is designed to have a configuration ensuring that the two heads step in the hand-over-hand rather than in the inchworm manner. The similarity between the two systems is that the directional movement is mainly *via* the Brownian ratchet mechanism whereas the NL docking plays an assistant role, as mentioned before for the dimer.[6,74] Thus, the studies here have strong implications not only for the mechanochemical coupling mechanism of the two coupled kinesin monomers but also for that of the single dimer.

It is mentioned here that we consider the simple case that the distance between the two connecting points of the stalk on the cargo is commensurate to the repeat period of tubulins on the MT filament and moreover consider implicitly that the stalk is connected fixedly to the cargo. In reality, the connection could not be fixed and two possible cases are present. (1) One case is that the stalk cannot slide on the cargo surface but can rotate elastically relative to the cargo in a small range of angle. For this case, considering that the stalk is capable of rotating freely in a large range of angle relative to the head[75] the pathway of the two coupled monomers with a short stalk and with the distance between the two stalk-cargo connecting points being incommensurate to the repeat period of tubulins on the MT filament is shown in Fig. S3.† The analysis of the dynamics for the two coupled monomers based on Fig. S3† is more complicated than that based on Fig. 1 and more parameters are required. (2) Another case is that the angle of the stalk relative to the cargo is kept fixed but the stalk can slide on the cargo surface in a small range of distance. For this case, the pathway of the two coupled monomers is similar to that shown in Fig. 1, but instead in Fig. 1a the system can be in three states: in one state the two monomers have docked NLs, in another state one monomer has a docked NL and the other one has an undocked NL, and in the third state the two monomers have undocked NLs. For this case, the analysis is also more complicated than that presented in this work. The analyses for the two cases will be performed in the future.

Finally, it is mentioned that the model for the two coupled kinesin monomers, which is applicable to the kinesin-1, -2 and -3 families here, can also be applicable to other families.

# Data availability

The author confirms that the data supporting the findings of this study are available within the article.

# Conflicts of interest

No conflict of interest exists.

## References

1 R. D. Vale, T. S. Reese and M. P. Sheetz, Identification of a novel force-generating protein, kinesin, involved in microtubule-based motility, *Cell*, 1985, **42**, 39–50.
2 N. Hirokawa, Kinesin and dynein superfamily proteins and the mechanism of organelle transport, *Science*, 1998, **279**, 519–526.
3 R. D. Vale, The molecular motor toolbox for intracellular transport, *Cell*, 2003, **112**, 467–480.
4 C. J. Lawrence, R. K. Dawe, K. R. Christie, *et al.*, A standardized kinesin nomenclature, *J. Cell Biol.*, 2004, **167**, 19–22.
5 A. B. Kolomeisky and M. E. Fisher, Molecular motors: a theorist's perspective, *Annu. Rev. Phys. Chem.*, 2007, **58**, 675–695.
6 P. Xie, Insight into the chemomechanical coupling mechanism of kinesin molecular motors, *Commun. Theor. Phys.*, 2021, **73**, 57601.
7 D. Chowdhury, Stochastic mechano-chemical kinetics of molecular motors: a multidisciplinary enterprise from a physicist's perspective, *Phys. Rep.*, 2013, **529**, 1–197.
8 K. Visscher, M. J. Schnitzer and S. M. Block, Single kinesin molecules studied with a molecular force clamp, *Nature*, 1999, **400**, 184–189.
9 M. Nishiyama, H. Higuchi and T. Yanagida, Chemomechanical coupling of the forward and backward steps of single kinesin molecules, *Nat. Cell Biol.*, 2002, **4**, 790–797.
10 N. J. Carter and R. A. Cross, Mechanics of the kinesin step, *Nature*, 2005, **435**, 308–312.
11 G. T. Shubeita, S. L. Tran, J. Xu, *et al.*, Consequences of motor copy number on the intracellular transport of kinesin-1-driven lipid droplets, *Cell*, 2008, **135**, 1098–1107.
12 A. G. Hendricks, E. L. F. Holzbaur and Y. E. Goldman, Force measurements on cargoes in living cells reveal collective dynamics of microtubule motors, *Proc. Natl. Acad. Sci. U. S. A.*, 2012, **109**, 18447–18452.
13 R. T. McLaughlin, M. R. Diehl and A. B. Kolomeisky, Collective dynamics of processive cytoskeletal motors, *Soft Matter*, 2016, **12**, 14–21.
14 S. Klumpp and R. Lipowsky, Cooperative cargo transport by several molecular motors, *Proc. Natl. Acad. Sci. U. S. A.*, 2005, **102**, 17284–17289.
15 J. W. Driver, D. K. Jamison, K. Uppulury, A. R. Rogers, A. B. Kolomeisky and M. R. Diehl, Productive cooperation among processive motors depends inversely on their mechanochemical efficiency, *Biophys. J.*, 2011, **101**, 386–395.
16 F. Berger, C. Keller, R. Lipowsky and S. Klumpp, Elastic coupling effects in cooperative transport by a pair of molecular motors, *Cell. Mol. Bioeng.*, 2013, **6**, 48–64.
17 D. Bhat and M. Gopalakrishnan, Stall force of a cargo driven by N interacting motor proteins, *Europhys. Lett.*, 2017, **117**, 28004.
18 T. Bameta, D. Das, D. Das, R. Padinhateeri and M. M. Inamdar, Sufficient conditions for the additivity of stall forces generated by multiple filaments or motors, *Phys. Rev. E*, 2017, **95**, 022406.
19 B. J. N. Reddy, S. Tripathy, M. Vershinin, *et al.*, Heterogeneity in kinesin function, *Traffic*, 2017, **18**, 658–671.
20 Q. Feng, K. J. Mickolajczyk, G.-Y. Chen and W. O. Hancock, Motor reattachment kinetics play a dominant role in multimotor-driven cargo transport, *Biophys. J.*, 2018, **114**, 400–409.
21 D. K. Jamison, J. W. Driver, A. R. Rogers, P. E. Constantinou and M. R. Diehl, Two kinesins transport cargo primarily *via* the action of one motor: implications for intracellular transport, *Biophys. J.*, 2010, **99**, 2967–2977.
22 J. C. Dallon, C. Leduc, S. Etienne-Manneville and S. Portet, Stochastic modeling reveals how motor protein and filament properties affect intermediate filament transport, *J. Theor. Biol.*, 2019, **464**, 132–148.
23 Y.-B. Fu, S.-K. Guo, P.-Y. Wang and P. Xie, Dynamics of cooperative cargo transport by two elastically coupled kinesin motors, *Eur. Phys. J. E: Soft Matter Biol. Phys.*, 2019, **42**, 41.
24 J. Xu, Z. Shu, S. J. King and S. P. Gross, Tuning multiple motor travel *via* single motor velocity, *Traffic*, 2012, **13**, 1198–1205.
25 N. D. Derr, B. S. Goodman, R. Jungmann, A. E. Leschziner, W. M. Shih and S. L. Reck-peterson, Tug-of-war in motor protein ensembles revealed with a programmable DNA origami scaffold, *Science*, 2012, **338**, 662–665.
26 K. Furuta, A. Furuta, Y. Y. Toyoshima, M. Amino, K. Oiwa and H. Kojima, Measuring collective transport by defined numbers of processive and nonprocessive kinesin motors, *Proc. Natl. Acad. Sci. U. S. A.*, 2013, **110**, 501–506.
27 S. Klumpp and R. Lipowsky, Cooperative cargo transport by several molecular motors, *Proc. Natl. Acad. Sci. U. S. A.*, 2005, **102**, 17284–17289.
28 Y. Wang, Y.-Y. Liu, J. Liang, P.-Y. Wang and P. Xie, Effects of rebinding rate and asymmetry in unbinding rate on cargo transport by multiple kinesin motors, *Commun. Theor. Phys.*, 2021, **73**, 015603.
29 E. Berliner, E. C. Young, K. Anderson, H. K. Mahtani and J. Gelles, Failure of a single-headed kinesin to track parallel to microtubule protofilaments, *Nature*, 1995, **373**, 718–721.
30 E. C. Young, H. K. Mahtani and J. Gelles, One-headed kinesin derivatives move by a nonprocessive, low-duty ratio mechanism unlike that of two-headed kinesin, *Biochemistry*, 1998, **37**, 3467–3479.
31 T. Kamei, S. Kakuta and H. Higuchi, Biased binding of single molecules and continuous movement of multiple molecules of truncated single-headed kinesin, *Biophys. J.*, 2005, **88**, 2068–2077.
32 M. R. Diehl, K. Zhang, H. J. Lee and D. A. Tirrell, Engineering cooperativity in biomotor-protein assemblies, *Science*, 2006, **311**, 1468–1471.
33 K. Nishinari, Y. Okada, A. Schadschneider and D. Chowdhury, Intracellular transport of single-headed molecular motors KIF1A, *Phys. Rev. Lett.*, 2005, **95**, 118101.

34 K. I. Schimert, B. G. Budaitis, D. N. Reinemann, M. J. Lang and K. J. Verhey, Intracellular cargo transport by single-headed kinesin motors, *Proc. Natl. Acad. Sci. U. S. A.*, 2019, **116**, 6152–6161.
35 J. Brugués and J. Casademunt, Self-organization and cooperativity of weakly coupled molecular motors under unequal loading, *Phys. Rev. Lett.*, 2009, **102**, 118104.
36 J. G. Orlandi, C. Blanch-Mercader, J. Brugués and J. Casademunt, Cooperativity of self-organized Brownian motors pulling on soft cargoes, *Phys. Rev. E: Stat., Nonlinear, Soft Matter Phys.*, 2010, **82**, 061903.
37 D. Oriola and J. Casademunt, Cooperative force generation of KIF1A Brownian motors, *Phys. Rev. Lett.*, 2013, **11**, 048103.
38 D. Oriola and J. Casademunt, Cooperative action of KIF1A Brownian motors with finite dwell time, *Phys. Rev. E: Stat., Nonlinear, Soft Matter Phys.*, 2014, **89**, 032722.
39 D. Oriola, S. Roth, M. Dogterom and J. Casademunt, Formation of helical membrane tubes around microtubules by single-headed kinesin KIF1A, *Nat. Commun.*, 2015, **6**, 8025.
40 P. Xie, S.-K. Guo and H. Chen, ATP-concentration- and force-dependent chemomechanical coupling of kinesin molecular motors, *J. Chem. Inf. Model.*, 2019, **59**, 360–372.
41 P. Xie, Non-tight and tight chemomechanical couplings of biomolecular motors under hindering loads, *J. Theor. Biol.*, 2020, **490**, 110173.
42 P. Xie, Theoretical analysis of dynamics of kinesin molecular motors, *ACS Omega*, 2020, **5**, 5721–5730.
43 I. M. T. C. Crevel, A. Lockhart and R. A. Cross, Weak and strong states of kinesin and Ncd, *J. Mol. Biol.*, 1996, **257**, 66–76.
44 H. Sosa, E. J. G. Peterman, W. E. Moerner and L. S. B. Goldstein, ADP-induced rocking of the kinesin motor domain revealed by single-molecule fluorescence polarization microscopy, *Nat. Struct. Biol.*, 2001, **8**, 540–544.
45 S. Uemura, K. Kawaguchi, J. Yajima, M. Edamatsu, Y. Y. Toyoshima and S. I. Ishiwata, Kinesin–microtubule binding depends on both nucleotide state and loading direction, *Proc. Natl. Acad. Sci. U. S. A.*, 2002, **99**, 5977–5981.
46 M. Morikawa, H. Yajima, R. Nitta, S. Inoue, T. Ogura, C. Sato and N. Hirokawa, X-ray and Cryo-EM Structures reveal mutual conformational changes of kinesin and GTP-state microtubules upon binding, *EMBO J.*, 2015, **34**, 1270–1286.
47 X.-X. Shi, Y.-B. Fu, S.-K. Guo, P.-Y. Wang, H. Chen and P. Xie, Investigating role of conformational changes of microtubule in regulating its binding affinity to kinesin by all-atom molecular dynamics simulation, *Proteins*, 2018, **86**, 1127–1139.
48 X.-X. Shi, P.-Y. Wang, H. Chen and P. Xie, Studies of conformational changes of tubulin induced by interaction with kinesin using atomistic molecular dynamics simulations, *Int. J. Mol. Sci.*, 2021, **22**, 6709.
49 K. J. Verhey and R. Ohi, Causes, costs and consequences of kinesin motors communicating through the microtubule lattice, *J. Cell Sci.*, 2023, **136**, jcs260735.
50 S. S. Wijeratne, S. A. Fiorenza, A. E. Neary, R. Subramanian and M. D. Betterton, Motor guidance by long-range communication on the microtubule highway, *Proc. Natl. Acad. Sci. U. S. A.*, 2022, **119**, e2120193119.
51 P. Xie, A model for cooperativity of kinesin-4 motors by communicating through the microtubule track, *Chem. Phys.*, 2024, **581**, 112274.
52 L. Cao, W. Wang, Q. Jiang, C. Wang, M. Knossow and B. Gigant, The structure of apo-kinesin bound to tubulin links the nucleotide cycle to movement, *Nat. Commun.*, 2014, **5**, 5364.
53 R. Nitta, Y. Okada and N. Hirokawa, Structural model for strain-dependent microtubule activation of Mg-ADP release from kinesin, *Nat. Struct. Mol. Biol.*, 2008, **15**, 1067–1075.
54 A. Yildiz, M. Tomishige, A. Gennerich and R. D. Vale, Intramolecular strain coordinates kinesin stepping behavior along microtubules, *Cell*, 2008, **134**, 1030–1041.
55 M. L. Moyer, S. P. Gilbert and K. A. Johnson, Pathway of ATP hydrolysis by monomeric and dimeric kinesin, *Biochemistry*, 1998, **37**, 800–813.
56 S. S. Rosenfeld, P. M. Fordyce, G. M. Jefferson, P. H. King and S. M. Block, Stepping and stretching: how kinesin uses internal strain to walk processively, *J. Biol. Chem.*, 2003, **278**, 18550–18556.
57 Y. Okada and N. Hirokawa, A processive single-headed motor: kinesin superfamily protein KIF1A, *Science*, 1999, **283**, 1152–1157.
58 S.-K. Guo, P.-Y. Wang and P. Xie, A model of processive movement of dimeric kinesin, *J. Theor. Biol.*, 2017, **414**, 62–75.
59 P. Xie, Modeling study of the dynamics of kinesin-14 molecular motors, *J. Phys. Chem. B*, 2022, **126**, 8720–8734.
60 P. Xie, Modeling processive motion of kinesin-13 MCAK and kinesin-14 Cik1-Kar3 molecular motors, *Protein Sci.*, 2021, **30**, 2092–2105.
61 C. Leduc, O. Campàs, K. B. Zeldovich, *et al.*, Cooperative extraction of membrane nanotubes by molecular motors, *Proc. Natl. Acad. Sci. U. S. A.*, 2004, **101**, 17096–17101.
62 S. Uemura, H. Higuchi, A. O. Olivares, E. M. De La Cruz and S. Ishiwata, Mechanochemical coupling of two substeps in a single myosin V motor, *Nat. Struct. Mol. Biol.*, 2004, **11**, 877–883.
63 S. Sudhakar, M. Kazem, A. Tobias, J. Jachowski, M. Bugiel, A. Jannasch and E. Schäffer, Germanium nanospheres for ultraresolution picotensiometry of kinesin motors, *Science*, 2021, **71**, eabd9944.
64 P. Xie, Effect of varying load in moving period of a step on dynamics of molecular motors, *Eur. Phys. J. E: Soft Matter Biol. Phys.*, 2022, **45**, 28.
65 S. Rice, Y. Cui, C. Sindelar, N. Naber, M. Matuska, R. Vale and R. Cooke, Thermodynamic properties of the kinesin neck region docking to the catalytic core, *Biophys. J.*, 2003, **84**, 1844–1854.
66 W. Hwang, M. J. Lang and M. Karplus, Kinesin motility is driven by subdomain dynamics, *eLife*, 2017, **6**, e28948.
67 H. Isojima, R. Iino, Y. Niitani, H. Noji and M. Tomishige, Direct observation of intermediate states during the stepping motion of kinesin-1, *Nat. Chem. Biol.*, 2016, **12**, 290–297.

68 P. Xie, ATP-concentration-dependent fractions of one-head-bound and two-heads-bound states of kinesin motor during its chemomechanical coupling cycle, *J. Phys. Chem. Lett.*, 2024, **15**, 3893–3899.
69 C. M. Coppin, D. W. Pierce, L. Hsu and R. D. Vale, The load dependence of kinesin's mechanical cycle, *Proc. Natl. Acad. Sci. U. S. A.*, 1997, **94**, 8539–8544.
70 S. Jeney, E. H. K. Stelzer, H. Grubmuller and E. L. Florin, Mechanical properties of single motor molecules studied by three-dimensional thermal force probing in optical tweezers, *ChemPhysChem*, 2004, **5**, 1150–1158.
71 J. O. L. Andreasson, S. Shastry, W. O. Hancock and S. M. Block, The mechanochemical cycle of mammalian kinesin-2 KIF3A/B under load, *Curr. Biol.*, 2015, **25**, 1166–1175.
72 B. M. Bensel, M. S. Woody, S. Pyrpassopoulos, Y. E. Goldman, S. P. Gilbert and E. M. Ostap, The mechanochemistry of the kinesin-2 KIF3AC heterodimer is related to strain-dependent kinetic properties of KIF3A and KIF3C, *Proc. Natl. Acad. Sci. U. S. A.*, 2020, **117**, 15632–15641.
73 P. Xie, A model for chemomechanical coupling of kinesin-3 motor, *Cell. Mol. Bioeng.*, 2024, **17**, 137–151.
74 P. Xie, Effect of the neck linker on processive stepping of kinesin motor, *Biophysica*, 2023, **3**, 46–68.
75 Y. Wang, Y.-R. Liu, P.-Y. Wang and P. Xie, Dynamics of cooperative transport by multiple kinesin motors and diffusing microtubule-associated proteins, *Commun. Theor. Phys.*, 2022, **74**, 105601.